SANDIA REPORT SAND81-2615 • Unlimited Release • UC-70
Printed April 1982

Reprinted November 1983

A Continuum Description for Jointed Media

Robert K. Thomas

Prepared by
Sandia National Laboratories
Albuquerque, New Mexico 87185 and Livermore, California 94550
for the United States Department of Energy
under Contract DE-AC04-76DP00789

Issued by Sandia National Laboratories, operated for the United States Department of Energy by Sandia Corporation.

Printed in the United States of America
Available from
National Technical Information Service
U.S. Department of Commerce
5285 Port Royal Road
Springfield, VA 22161

NTIS price codes
Printed copy: A02
Microfiche copy: A01

SAND81-2615
Unlimited Release
Printed April 1982

Distribution
Category UC-70

A Continuum Description for Jointed Media*

Robert K. Thomas
Applied Mechanics Division I, 5521
Sandia National Laboratories**
Albuquerque, NM 87185

Abstract

A general three-dimensional continuum description is presented for a material containing regularly spaced and approximately parallel jointing planes within a representative elementary volume. Constitutive relationships are introduced for linear behavior of the base material and nonlinear normal and shear behavior across jointing planes. Furthermore, a fracture permeability tensor is calculated so that deformation induced alterations to the in-situ values can be measured. Examples for several strain-controlled loading paths are presented.

*This work was supported by the US Department of Energy (DOE) under contract DE-AC04-76-DP00789.
**A US DOE facility.

Contents

Figures

A Continuum Description for Jointed Media

Introduction

This report presents a general three-dimensional material model for regularly jointed media. The model is composed of two parts: a continuum approximation based on average discontinuous displacements across jointing planes within a representative elementary volume, and a material constitutive description based on linear behavior of the base material and nonlinear normal and shear behavior between jointing planes. Standard relationships for the balance laws have been adopted. All material constants can be obtained by laboratory measurements on single-joint specimens.

The specific application of the material model presented in this report is underground disposal of nuclear waste in a hard-rock geologic medium. This work is part of the Nevada Nuclear Waste Storage Investigations (NNWSI) administered by the Nevada Operations Office (NVO) of the U.S. Department of Energy (DOE). For these problems, the medium is usually highly jointed and the repository horizon is either partially saturated above the water table or fully saturated below the water table. Since the instantaneous fracture permeability is governed primarily by the deformation response, a material description that contains explicit discontinuous normal and shear displacements across the jointing planes is needed. A section of this report is devoted to the construction of a fracture permeability tensor based on the same continuum approximation. It is hoped, however, that this material model will be useful in other applications where the medium is anisotropic because of regular jointing, such as the response of underground structures during blast or earthquake loading.

Continuum theory may not necessarily be the best approach for modeling certain jointed rock masses. Studies are currently underway to characterize rock masses as to whether a homogeneous continuum theory is applicable and, if so, to determine the smallest representative elementary volume for modeling.[1] Network theory and statistical methods are used in these studies. If the representative elementary volume is unsuitably large, then discrete joint models are necessary. Clearly, both continuum models and discrete joint models are required to satisfactorily analyze large scale geotechnical problems where major discontinuities such as faults and dikes are present.

Continuum Approximation

The continuum model in this report is based upon the published work of Morland.[2-4] Consider a "representative elementary volume" containing regularly spaced and parallel fractures as sketched in Figure 1. The orientation of this joint set is characterized by a unit normal vector $\underset{\sim}{n}$ with respect to fixed x_1, x_2, x_3 coordinate axes. The spacing between fractures is denoted by δ. Additional unit vectors $\underset{\sim}{s}$ and $\underset{\sim}{t}$ in the plane of the fractures are introduced such that $\underset{\sim}{s}$, $\underset{\sim}{t}$, $\underset{\sim}{n}$ form a local orthogonal coordinate system. These vectors are constructed such that $\underset{\sim}{s}$ lies in the x_1, x_2 plane, and $\underset{\sim}{t}$ points in the positive x_3 direction.

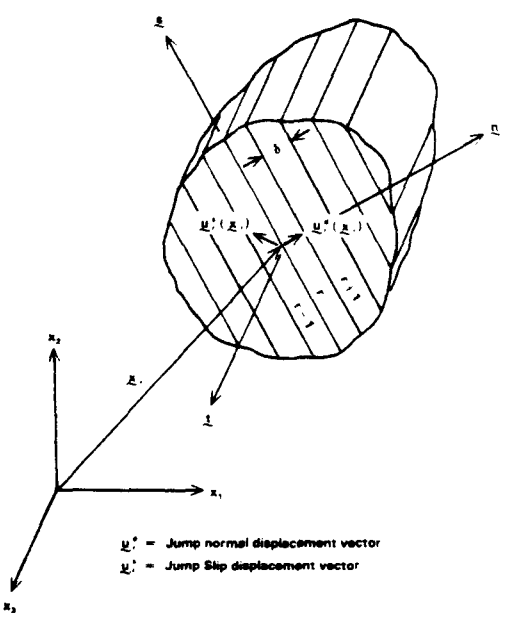

Figure 1. A Representative Elementary Volume Containing Regularly Spaced and Parallel Fractures Separated by a Distance δ

It is assumed that the relative motion between interfaces of the r^{th} fracture at the position $\underset{\sim}{x}_r$ can be measured by a jump "dilation" displacement vector $\underset{\sim}{u}^d_r(\underset{\sim}{x}_r)$ normal to the fracture plane, and a jump "slip" displacement vector $\underset{\sim}{u}^s_r(\underset{\sim}{x}_r)$ parallel to the fracture plane. The net jump displacements, for R fractures in the representative elementary volume, will then be

$$R\underset{\sim}{\bar{u}}^d(\underset{\sim}{x}) = \sum_{r=1}^{R} \underset{\sim}{u}^d_r(\underset{\sim}{x}_r)$$

$$R\underset{\sim}{\bar{u}}^s(\underset{\sim}{x}) = \sum_{r=1}^{R} \underset{\sim}{u}^s_r(\underset{\sim}{x}_r) \tag{1}$$

where $\underset{\sim}{\bar{u}}^d$ and $\underset{\sim}{\bar{u}}^s$ are average displacements, and $\underset{\sim}{x}$ is any position within the element. The characteristic dimension of the representative elementary volume is $R\delta$. As $R\delta$ tends to zero, or becomes small compared to the length scales of interest, the individual discontinuities will be unimportant provided that the correct net jump displacements are measured. On this basis, continuous displacement fields $\underset{\sim}{u}^d$ and $\underset{\sim}{u}^s$ with respect to the fixed x_1, x_2, x_3 coordinate axes are introduced,

$$\underset{\sim}{u}^d(\underset{\sim}{x} + d\underset{\sim}{n}) = \underset{\sim}{u}^d(\underset{\sim}{x}) + \left(\frac{\bar{u}^d}{\delta}\right)d\underset{\sim}{n}$$

$$\underset{\sim}{u}^s(\underset{\sim}{x} + d\underset{\sim}{n}) = \underset{\sim}{u}^s(\underset{\sim}{x}) + \left(\frac{\bar{u}^s}{\delta}\right)d\underset{\sim}{n}, \tag{2}$$

where

$$\underset{\sim}{\bar{u}}^d = |\underset{\sim}{\bar{u}}^d|\,\underset{\sim}{n} = \bar{u}^d\,\underset{\sim}{n}$$

$$\underset{\sim}{\bar{u}}^s = |\underset{\sim}{\bar{u}}^s|\,\underset{\sim}{v} = \bar{u}^s\,\underset{\sim}{v} \tag{3}$$

In Eq (3), the direction of the slip displacement is in the direction of the unit vector $\underset{\sim}{v}$, which lies in the $\underset{\sim}{s}$, $\underset{\sim}{t}$, plane and is normal to $\underset{\sim}{n}$. The total displacements can be written as the decomposition,

$$\underset{\sim}{u}(\underset{\sim}{x}) = \underset{\sim}{u}^c(\underset{\sim}{x}) + \underset{\sim}{u}^d(\underset{\sim}{x}) + \underset{\sim}{u}^s(\underset{\sim}{x}) \tag{4}$$

where $\underset{\sim}{u}^c$ is a continuous displacement field.

Equation (4) suggests a strain decomposition of the form,

$$\underset{\approx}{\varepsilon}(\underset{\sim}{x}) = \underset{\approx}{\varepsilon}^c(\underset{\sim}{x}) + \underset{\approx}{\varepsilon}^d(\underset{\sim}{x}) + \underset{\approx}{\varepsilon}^s(\underset{\sim}{x}) \tag{5}$$

However, in the absence of a fracture set,

$$\underset{\approx}{\varepsilon} = \underset{\approx}{\varepsilon}^b, \tag{6}$$

where $\underset{\approx}{\varepsilon}^b$ is the strain associated with the intact material between fractures and is called the block strain. On this basis, the strain decomposition is taken to be,

$$\underset{\approx}{\varepsilon} = \underset{\approx}{\varepsilon}^b + \underset{\approx}{\varepsilon}^d + \underset{\approx}{\varepsilon}^s \tag{7}$$

The dilation and slip strains are defined in terms of the continuous displacements,

$$2\underset{\approx}{\varepsilon}^d = \underset{\sim}{u}^d\nabla + (\underset{\sim}{u}^d\nabla)^T$$

$$2\underset{\approx}{\varepsilon}^s = \underset{\sim}{u}^s\nabla + (\underset{\sim}{u}^s\nabla)^T \tag{8}$$

where ∇ is the gradient operator with respect to the fixed x_1, x_2, x_3 axes. Equation (8) can be reduced to a more useful form. Decompose $\underset{\sim}{u}^d$ and $\underset{\sim}{u}^s$ into components in the local coordinate system,

$$\underset{\sim}{u}^d = |\underset{\sim}{u}^d|\,\underset{\sim}{n} = u^d\,\underset{\sim}{n}$$

$$\underset{\sim}{u}^s = |\underset{\sim}{u}^s|\,\underset{\sim}{v} = u^s_s\,\underset{\sim}{s} + u^s_t\,\underset{\sim}{t} \tag{9}$$

Within the representative elementary volume, both $\underset{\sim}{u}^d$ and $\underset{\sim}{u}^s$ have nonzero gradients only in the direction normal to the fracture planes. Thus Eq (8) becomes

$$\underset{\approx}{\varepsilon}^d = \frac{\partial u^d}{\partial n}(\underset{\sim}{n} \otimes \underset{\sim}{n})$$

$$\underset{\approx}{\varepsilon}^s = \frac{1}{2}\frac{\partial u^s_s}{\partial n}(\underset{\sim}{s} \otimes \underset{\sim}{n} + \underset{\sim}{n} \otimes \underset{\sim}{s}) + \frac{1}{2}\frac{\partial u^s_t}{\partial n}(\underset{\sim}{t} \otimes \underset{\sim}{n} + \underset{\sim}{n} \otimes \underset{\sim}{t}), \tag{10}$$

where n is a coordinate in the direction $\underset{\sim}{n}$. From Eq (2),

$$\frac{\partial u^d}{\partial n} = \frac{\bar{u}^d}{\delta}$$

$$\frac{\partial u^s}{\partial n} = \frac{\bar{u}^s}{\delta} \tag{11}$$

so the final form for the strains is

$$\underset{\approx}{\varepsilon}^{d} = \frac{u^{d}}{\delta}\,(\underset{\sim}{n} \otimes \underset{\sim}{n})$$

$$\underset{\approx}{\varepsilon}^{s} = \frac{u_{s}}{2\delta}\,(\underset{\sim}{s} \otimes \underset{\sim}{n} + \underset{\sim}{n} \otimes \underset{\sim}{s}) + \frac{u_{t}}{2\delta}\,(\underset{\sim}{t} \otimes \underset{\sim}{n} + \underset{\sim}{n} \otimes \underset{\sim}{t})\,. \qquad (12)$$

In Eq (12) the fracture spacing δ and the average jump displacements u^{d} and u^{s} are explicit in the continuous strain approximation.

Constitutive Model

It will prove useful to introduce the components of a stress tensor $\underset{\approx}{T}$ and the components of a total strain tensor $\underset{\approx}{E}$ which refer to the local $\underset{\sim}{s}$, $\underset{\sim}{t}$, $\underset{\sim}{n}$ coordinate system. If $\underset{\approx}{\sigma}$ and $\underset{\approx}{\varepsilon}$ are stress and strain tensors that refer to fixed x_1, x_2, x_3 axes, then the transformation equations are

$$\begin{aligned} T_{nn} &= \underset{\approx}{\sigma}\,\underset{\sim}{n}\cdot\underset{\sim}{n} & T_{ns} &= \underset{\approx}{\sigma}\,\underset{\sim}{n}\cdot\underset{\sim}{s} \\ T_{ss} &= \underset{\approx}{\sigma}\,\underset{\sim}{s}\cdot\underset{\sim}{s} & T_{st} &= \underset{\approx}{\sigma}\,\underset{\sim}{s}\cdot\underset{\sim}{t} \\ T_{tt} &= \underset{\approx}{\sigma}\,\underset{\sim}{t}\cdot\underset{\sim}{t} & T_{tn} &= \underset{\approx}{\sigma}\,\underset{\sim}{t}\cdot\underset{\sim}{n}, \end{aligned} \qquad (13)$$

and

$$\begin{aligned} E_{nn} &= \underset{\approx}{\varepsilon}\,\underset{\sim}{n}\cdot\underset{\sim}{n} & E_{ns} &= \underset{\approx}{\varepsilon}\,\underset{\sim}{n}\cdot\underset{\sim}{s} \\ E_{ss} &= \underset{\approx}{\varepsilon}\,\underset{\sim}{s}\cdot\underset{\sim}{s} & E_{st} &= \underset{\approx}{\varepsilon}\,\underset{\sim}{s}\cdot\underset{\sim}{t} \\ E_{tt} &= \underset{\approx}{\varepsilon}\,\underset{\sim}{t}\cdot\underset{\sim}{t} & E_{tn} &= \underset{\approx}{\varepsilon}\,\underset{\sim}{t}\cdot\underset{\sim}{n}\,. \end{aligned} \qquad (14)$$

For a fracture set with normal $\underset{\sim}{n}$, the normal stress is T_{nn}, and the shear stresses are T_{ns} and T_{nt}. The shear stress vector acting on this plane is

$$\underset{\sim}{\tau} = \underset{\approx}{\sigma}\,\underset{\sim}{n} - (\underset{\approx}{\sigma}\,\underset{\sim}{n}\cdot\underset{\sim}{n})\,\underset{\approx}{I}\,\underset{\sim}{n}\,, \qquad (15)$$

and the shear strain vector is

$$\underset{\sim}{\gamma} = \underset{\approx}{\varepsilon}\,\underset{\sim}{n} - (\underset{\approx}{\varepsilon}\,\underset{\sim}{n}\cdot\underset{\sim}{n})\,\underset{\approx}{I}\,\underset{\sim}{n}\,. \qquad (16)$$

Intact Material

In the present formulation, the intact material is assumed to behave as a linear elastic solid; i.e., the block strain rate is

$$\dot{\underset{\approx}{\varepsilon}}^{b} = \frac{\dot{\underset{\approx}{\sigma}}}{2G} - \left(\frac{K - \frac{2}{3}G}{6KG}\right)(\mathrm{tr}\,\dot{\underset{\approx}{\sigma}})\,\underset{\approx}{I}\,. \qquad (17)$$

Joint Dilation

Laboratory data have shown that the stress-displacement relationship for motion normal to a joint plane is highly nonlinear. Initially, when two fracture planes are brought together, the actual surface area in contact is almost zero. The entire normal force is sustained by three or more contact points. As the normal load increases, the point contacts enlarge by elastic deformation and then plastic crushing. An empirical approach is taken here based on discrete joint models that are discussed by Goodman[5] and shown in Figure 2. First, an open joint has no tensile strength, so

$$T_{nn} = 0,\ u^{d} \geq 0\,. \qquad (18)$$

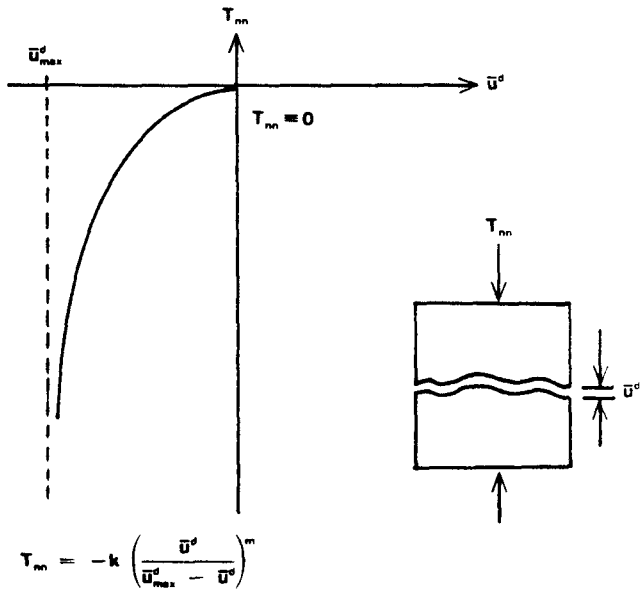

Figure 2. Assumed Joint Stiffness Behavior Normal to a Single Joint Plane

Second, there is a limit to the amount of compression possible, and at this limit the joint stiffness is infinite. A general power-law relationship describing this behavior is assumed here,

$$T_{nn} = -k\left(\frac{u^{d}}{u^{d}_{max} - u^{d}}\right)^{m}, \qquad u^{d} < 0\,, \qquad (19)$$

where k and m are constants and u^d_{max} is the maximum closure. These constants are determined from laboratory experiments on single-joint specimens. It follows that the rate equation is

$$\dot{u}^d = f' \dot{T}_{nn}$$

$$= -\frac{1}{km}\left[\frac{(u^d_{max} - u^d)^2}{u^d_{max}}\right]\left(\frac{u^d_{max} - u^d}{u^d}\right)^{m-1} \dot{T}_{nn} \quad (20)$$

From Eq (12) and (20) the dilation strain rate is

$$\underset{\approx}{\dot{e}}^d = \frac{f'}{\delta} \dot{T}_{nn} (\underset{\sim}{n} \otimes \underset{\sim}{n}) \quad (21)$$

Although joint compression may be largely irreversible, it is assumed to be nonlinear elastic in this report.

Joint Shear

The joint shear stress-displacement behavior is assumed to be elastic and perfectly plastic. In the elastic range

$$\dot{u}^s_s = \frac{\dot{T}_{ns}}{G_s}, \dot{u}^s_t = \frac{\dot{T}_{nt}}{G_s}, \quad (22)$$

where G_s is a constant to be determined from single-joint laboratory data. From Eq (12) the slip strain rate is

$$\underset{\sim}{\dot{e}}^s = \frac{\dot{T}_{ns}}{2\delta G_s}(\underset{\sim}{s} \otimes \underset{\sim}{n} + \underset{\sim}{n} \otimes \underset{\sim}{s})$$

$$+ \frac{\dot{T}_{nt}}{2\delta G_s}(\underset{\sim}{t} \otimes \underset{\sim}{n} + \underset{\sim}{n} \otimes \underset{\sim}{t}) . \quad (23)$$

The onset of plastic behavior is assumed to be governed by a linear Mohr-Coulomb criterion. Based on a scalar "slip function" defined by,

$$F = |\underset{\sim}{\tau}| + \mu T_{nn} - Co, \quad (24)$$

where μ is the friction coefficient and Co is the cohesion, the joint behavior is elastic for $F \leq 0$ and plastic for $F > 0$. With Eq (13) and (15), the slip function in Eq (24) can be written in the more general form,

$$F = |\underset{\approx}{\sigma}\underset{\sim}{n} - (\underset{\approx}{\sigma}\underset{\sim}{n} \cdot \underset{\sim}{n})\underset{\sim}{n}| + \mu \underset{\approx}{\sigma}\underset{\sim}{n} \cdot \underset{\sim}{n} - Co. \quad (25)$$

Coupled Dilation Displacements

It is well established that, in a direct shear test with constant normal stress, the dilation displacement of a jointed specimen increases as the shear displacement increases. This phenomenon is called a coupled-dilation displacement, and it is caused by fracture interfaces rolling over asperities. It is more pronounced at low normal stresses than at high normal stresses. A coupled shear displacement, caused by pure uniaxial loading normal to a joint plane, is ruled out by the invariance requirements on the constitutive equations. In this report we assume the following joint flexibility equations:

$$u^d = f(T_{nn}) + |\underset{\sim}{u}^s| \tan \psi$$

$$u^s_s = T_{ns}/G_s$$

$$u^s_t = T_{nt}/G_s , \quad (26)$$

where the function f is defined in Eq (19). This behavior is shown in Figure 3. The coupled dilation is a linear function of the shear displacement with the proportionality constant equal to $\tan \psi$. The effective shear displacement $|\underset{\sim}{u}^s|$ is equal to the magnitude of the shear displacement in the $\underset{\sim}{s}$, $\underset{\sim}{t}$ plane, and its direction is the same as the direction of the maximum shear stress $|\underset{\sim}{\tau}|$ in this plane. Furthermore, from Eq (26),

$$|\underset{\sim}{u}^s| = |\underset{\sim}{\tau}|/G_s . \quad (27)$$

At a shear displacement of u_p (in Figure 3), the coupled dilation effect ceases due to incipient shear slippage. From Eq (26) and (27) the rate equation for the dilation displacement is

$$\dot{u}^d = f' \dot{T}_{nn} + \frac{\tan \psi}{G_s}|\dot{\underset{\sim}{\tau}}| , \quad (28)$$

and from Eq (12) the dilation strain rate is

$$\underset{\approx}{\dot{e}}^d = \left(\frac{f' \dot{T}_{nn}}{\delta} + \frac{\tan \psi}{\delta G_s}|\dot{\underset{\sim}{\tau}}|\right)(\underset{\sim}{n} \otimes \underset{\sim}{n}) . \quad (29)$$

The rate equation for slip remains unchanged from Eq (22).

The coupled dilation displacement is viewed as being reversible in the elastic preslip range; i.e., for $|\underset{\sim}{u}^s| \leq u_p$ in Figure 3. This appears to be a realistic

assumption since crushing and shearing of asperities does not take place to a significant extent in this range. When unloading occurs, the value of $|\dot{\underset{\sim}{\tau}}|$ in Eq (28) and (29) must be replaced by $-|\dot{\underset{\sim}{\tau}}|$. Unloading is detected by measuring $|\underset{\sim}{u}_s|$ in the $\underset{\sim}{s}$, $\underset{\sim}{t}$ plane. This method accurately tracks radial loading and unloading paths; a more general algorithm is required for other paths.

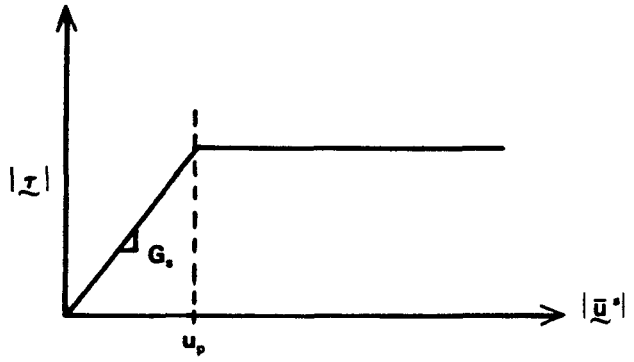

Figure 3a. Assumed Joint Stiffness Behavior in Shear Parallel to a Single Joint Plane

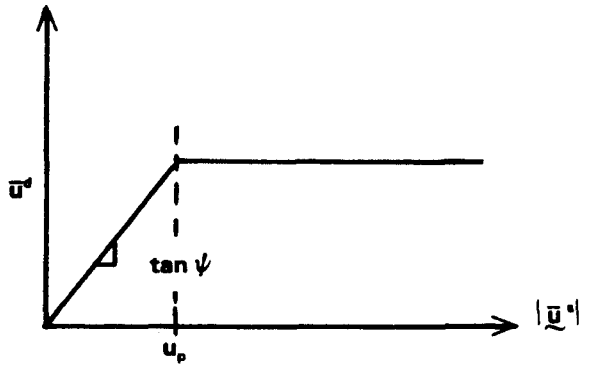

Figure 3b. Assumed Coupled Dilation Behavior for Normal and Shear Displacements

In the postslip range the coupled dilation displacement is thought to be only partially reversible; in this report, it is assumed to be totally irreversible. Once plastic slippage occurs, the dilation angle ψ is set to zero for all subsequent loading and unloading paths.

Solution of Constitutive Equations

Consider the general situation in incremental stress analysis where the stresses and strains are known at the last load step; the current strain rates are known, and it is desired to find the current stresses.

On the basis of Eq (7), decompose the total strain rate,

$$\dot{\underset{\approx}{\varepsilon}} = \dot{\underset{\approx}{\varepsilon}}^b + \dot{\underset{\approx}{\varepsilon}}^d + \dot{\underset{\approx}{\varepsilon}}^s_e + \dot{\underset{\approx}{\varepsilon}}^s_p \,. \tag{30}$$

The block strain is linear elastic, the dilation strain is nonlinear elastic, and the slip strain has been further decomposed into a linear elastic part and a perfectly plastic part. First, assume that plastic shearing does not occur, and proceed to calculate an elastic trial stress. With the constitutive relations in Eq (17), (23), and (29), the total strain rate [Eq (30)] becomes

$$\begin{aligned}\dot{\underset{\approx}{\varepsilon}} = {} & \frac{\dot{\underset{\approx}{\sigma}}}{2G} - \left(\frac{K - \frac{2}{3}G}{6KG}\right)(\mathrm{tr}\,\dot{\underset{\approx}{\sigma}})\,\underset{\approx}{I} \\ & + \left[\frac{f'}{\delta}\dot{T}_{nn} + \frac{\tan\psi}{\delta G_s}|\dot{\underset{\sim}{\tau}}|\right](\underset{\sim}{n}\otimes\underset{\sim}{n}) \\ & + \frac{\dot{T}_{ns}}{2\delta G_s}(\underset{\sim}{s}\otimes\underset{\sim}{n} + \underset{\sim}{n}\otimes\underset{\sim}{s}) \\ & + \frac{\dot{T}_{nt}}{2\delta G_s}(\underset{\sim}{t}\otimes\underset{\sim}{n} + \underset{\sim}{n}\otimes\underset{\sim}{t})\end{aligned} \tag{31}$$

It is convenient to transform Eq (31) to six scalar equations in terms of the six stress components acting parallel and perpendicular to the plane of the fractures. These equations are obtained by taking successive scalar products of each side of Eq (31) with $\underset{\sim}{n}$, $\underset{\sim}{s}$, and $\underset{\sim}{t}$:

$$\begin{aligned}\dot{E}_{nn} &= \frac{\dot{T}_{nn}}{2G} - \frac{K - \frac{2}{3}G}{6KG}(\mathrm{tr}\,\dot{\underset{\approx}{T}}) + \frac{f'}{\delta}\dot{T}_{nn} + \frac{\tan\psi}{\delta G_s}|\dot{\underset{\sim}{\tau}}| \\ \dot{E}_{ns} &= \left(\frac{1}{2G} + \frac{1}{2\delta G_s}\right)\dot{T}_{ns} \\ \dot{E}_{nt} &= \left(\frac{1}{2G} + \frac{1}{2\delta G_s}\right)\dot{T}_{nt} \\ \dot{E}_{ss} &= \frac{\dot{T}_{ss}}{2G} - \frac{K - \frac{2}{3}G}{6KG}(\mathrm{tr}\,\dot{\underset{\approx}{T}}) \\ \dot{E}_{tt} &= \frac{\dot{T}_{tt}}{2G} - \frac{K - \frac{2}{3}G}{6KG}(\mathrm{tr}\,\dot{\underset{\approx}{T}}) \\ \dot{E}_{st} &= \frac{\dot{T}_{st}}{2G}\end{aligned} \tag{32}$$

in which the strain-rate components are defined by Eq (14). The shear stress rates can be obtained directly,

$$\dot{T}_{ns} = \left(\frac{2G}{1+\frac{G}{\delta G_s}}\right)\dot{E}_{ns}$$

$$\dot{T}_{nt} = \left(\frac{2G}{1+\frac{G}{\delta G_s}}\right)\dot{E}_{nt}$$

$$\dot{T}_{st} = (2G)\,\dot{E}_{st} \tag{33}$$

With the incremental shear stresses, the incremental direct stresses are obtained by the following calculational sequence:

$$|\dot{\underset{\sim}{\tau}}| = (\dot{T}_{ns}^2 + \dot{T}_{nt}^2)^{1/2}$$

$$\dot{T}_{nn} = \frac{2G\dot{E}_{nn} + \left(K - \frac{2}{3}G\right)\mathrm{tr}\,\dot{\underset{\approx}{E}} - \left(K + \frac{4}{3}G\right)\frac{\tan\psi}{\delta G_s}|\dot{\underset{\sim}{\tau}}|}{1 + \left(K+\frac{4}{3}G\right)\frac{f'}{\delta}}$$

$$\mathrm{tr}\,\dot{\underset{\approx}{T}} = 3K\left[\mathrm{tr}\,\dot{\underset{\approx}{E}} - \frac{f'}{\delta}\dot{T}_{nn} - \frac{\tan\psi}{\delta G_s}|\dot{\underset{\sim}{\tau}}|\right]$$

$$\dot{T}_{ss} = 2G\,\dot{E}_{ss} + \frac{K - \frac{2}{3}G}{3K}\mathrm{tr}\,\dot{\underset{\approx}{T}}$$

$$\dot{T}_{tt} = 2G\,\dot{E}_{tt} + \frac{K - \frac{2}{3}G}{3K}\mathrm{tr}\,\dot{\underset{\approx}{T}} \tag{34}$$

The stress rates in Eq (34) are not obtained directly because the secant stiffnesses are nonlinear functions of the normal stress T_{nn}. Rapid convergence, however, is achieved in very few iterations.

The current elastic trial stress is obtained by updating the previous stress with the incremental stresses. The next step is to check the slip function [Eq (25)]. If $F \leq 0$, then indeed the strain rate was entirely elastic and the current stress-rate components are given by Eq (33) and (34). However, if $F > 0$, then plastic slip has occurred and further calculations are necessary.

Assume a flow rule for the plastic slip strain rate of the form

$$\dot{\underset{\approx}{e}}_p^s = \lambda(\underset{\sim}{v} \otimes \underset{\sim}{n} + \underset{\sim}{n} \otimes \underset{\sim}{v}) \tag{35}$$

where λ is a constant, and $\underset{\sim}{v}$ is a unit vector in the direction of slip and is determined from the shear stress rate acting on the fracture plane; i.e.,

$$\dot{\underset{\sim}{\tau}} = |\dot{\underset{\sim}{\tau}}|\,\underset{\sim}{v} = \dot{\tau}\,\underset{\sim}{v}. \tag{36}$$

The flow rule in Eq (35) is nonassociative, and implies that the plastic slip strain rate is not normal to the loading surface [Eq (25)], but rather lies in the direction of the shear stress rate acting in the plane of the joint. From Eq (25) the consistency condition is

$$\dot{F} = |\dot{\underset{\approx}{\sigma}}\,\underset{\sim}{n} - (\dot{\underset{\approx}{\sigma}}\,\underset{\sim}{n}\cdot\underset{\sim}{n})\,\underset{\approx}{I}\,\underset{\sim}{n}| + \mu\,\dot{\underset{\approx}{\sigma}}\,\underset{\sim}{n}\cdot\underset{\sim}{n} = 0. \tag{37}$$

Consider a linear stress rate

$$\dot{\underset{\approx}{\sigma}} = \underset{\approx\approx}{c}^*(\dot{\underset{\approx}{\varepsilon}} - \dot{\underset{\approx}{e}}_p^s)$$

$$= \underset{\approx\approx}{c}^*[\dot{\underset{\approx}{\varepsilon}} - \lambda(\underset{\sim}{v} \otimes \underset{\sim}{n} + \underset{\sim}{n} \otimes \underset{\sim}{v})] \tag{38}$$

where $\underset{\approx\approx}{c}^*$ is a fourth-order tensor of material secant stiffness, and substitute into the consistency condition Eq (37). This yields

$$|\dot{\underset{\approx}{\varepsilon}}\,\underset{\sim}{n} - (\dot{\underset{\approx}{\varepsilon}}\,\underset{\sim}{n}\cdot\underset{\sim}{n})\,\underset{\approx}{I}\,\underset{\sim}{n} - \lambda\underset{\sim}{v}| + \mu\,\dot{\underset{\approx}{\varepsilon}}\,\underset{\sim}{n}\cdot\underset{\sim}{n} = 0. \tag{39}$$

With the use of the definitions Eq (14) and (16), Eq (39) reduces to

$$|\dot{\underset{\sim}{\gamma}} - \lambda\underset{\sim}{v}| + \mu\,\dot{E}_{nn} = 0\,. \tag{40}$$

Since the shear strain-rate vector $|\dot{\underset{\sim}{\gamma}}|$ acting in the plane of jointing is in the same direction as the shear stress-rate vector $|\dot{\underset{\sim}{\tau}}|$, i.e.,

$$\dot{\underset{\sim}{\gamma}} = |\dot{\underset{\sim}{\gamma}}|\,\underset{\sim}{v} = \dot{\gamma}\,\underset{\sim}{v}\,, \tag{41}$$

it follows from Eq (40) that

$$\lambda = \dot{\gamma} + \mu\,\dot{E}_{nn}\,. \tag{42}$$

With λ known, the plastic strain rate can be determined from Eq (35), and new stress-rate components can be calculated by repeating Eq (33) and (34), but with the elastic strain rate derated as in Eq (38). The previous stresses are updated by the incremental stresses to obtain the current stresses. Again, the slip function is evaluated and it may be found that the current stresses still do not lie on the loading surface. An iterative procedure that converges rapidly to yield the correct stresses is a secant method that finds the λ giving a zero-valued slip function F.

Fracture Permeability Tensor

Consider now the construction of a permeability tensor for the same continuum approximation as proposed in the mechanical model. This derivation is taken from Neuman.[6] A sketch of the representative elementary volume is shown in Figure 4. The true steady-state velocity in the $\underset{\sim}{s}$ direction is approximated by Couette flow between parallel plates,

$$\underset{\sim}{V} = -\left(\frac{\rho g}{\mu}\right)\xi\,|\mathfrak{u}^d_{max} - \mathfrak{u}^d|^2\,(h\nabla \cdot \underset{\sim}{s})\,\underset{\sim}{s} \tag{43}$$

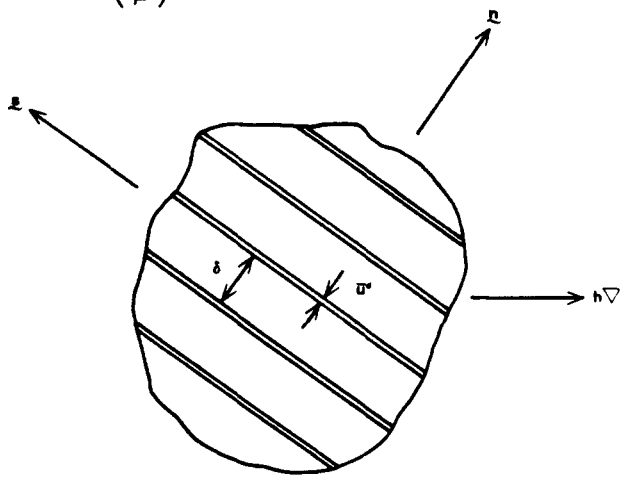

$\underset{\sim}{n}$ = Unit vector normal to joint planes
$\mathfrak{u}^d$ = Average joint aperature
δ = Average joint spacing
$h\nabla$ = Hydraulic gradient

Figure 4. Parallel Plate Approximation for Computation of a Fracture Permeability Tensor

where ξ is a surface roughness coefficient. The specific flux through the element, however, is

$$\underset{\sim}{q} = \phi\underset{\sim}{V} = \frac{|\mathfrak{u}^d_{max} - \mathfrak{u}^d|}{\delta}\underset{\sim}{V} \tag{44}$$

where ϕ is the porosity. Combining with Eq (43),

$$\underset{\sim}{q} = -\left(\frac{\rho g}{\mu}\right)\xi\,\frac{|\mathfrak{u}^d_{max} - \mathfrak{u}^d|^3}{\delta}\,(h\nabla \cdot \underset{\sim}{s})\,\underset{\sim}{s} \tag{45}$$

For consistency with the mechanical formulation, it is more convenient to describe the permeability tensor in terms of the unit normal vector $\underset{\sim}{n}$. From Figure 4,

$$\begin{aligned}(h\nabla\cdot\underset{\sim}{s})\,\underset{\sim}{s} &= h\nabla - (h\nabla\cdot\underset{\sim}{n})\,\underset{\sim}{n}\\ &= h\nabla - (\underset{\sim}{n}\otimes\underset{\sim}{n})h\nabla\\ &= (\underset{\approx}{I} - \underset{\sim}{n}\otimes\underset{\sim}{n})h\nabla\,.\end{aligned} \tag{46}$$

Now, for generalized Darcy flow,

$$\underset{\sim}{q} = -\left(\frac{\rho g}{\mu}\right)\underset{\approx}{k}\,h\nabla\,, \tag{47}$$

so it follows from Eq (45) and (46) that the permeability tensor is

$$\underset{\approx}{k} = \frac{\xi}{\delta}\,|\mathfrak{u}^d_{max} - \mathfrak{u}^d|^3\,(\underset{\approx}{I} - \underset{\sim}{n}\otimes\underset{\sim}{n}). \tag{48}$$

In Eq (48) the permeability is proportional to the third power of the joint aperature. It follows that an accurate laboratory measurement of joint normal stiffness is required to adequately address the flow problem. Also, the joint spacing and the average jump dilation displacement are explicit in the construction of the permeability tensor, just as these quantities were explicit in the construction of the strain tensors [Eq (12)].

Examples

The material properties used in the following examples were selected somewhat arbitrarily, but they are not unrealistically different from the properties of many common hard-rock masses.

Dilation Response

Consider the reduced problem,

$$e_{11} = e_{33} = e_{12} = e_{23} = e_{31} = 0$$

with the only nonzero strain being e_{22}. If

$$\underset{\sim}{n} = (0,1,0)^T,$$

then the stress σ_{22} measures the response to strains normal to the jointing planes as shown in Figure 5. Assume a stress-displacement relationship for a single joint,

$$\begin{aligned}k &= 1000 \text{ psi}\\ m &= 1.5\\ \mathfrak{u}^d_{max} &= -0.003 \text{ in.}\end{aligned}$$

which is plotted in Figure 6. For the intact rock,

$$\begin{aligned}K &= 0.667 \times 10^6 \text{ psi}\\ G &= 0.4 \times 10^6 \text{ psi}\end{aligned}$$

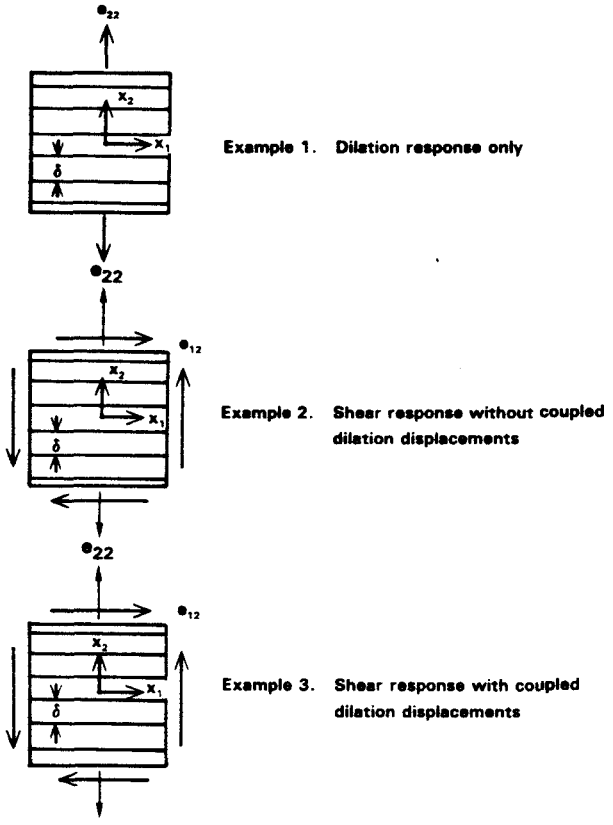

Figure 5. Strain-Controlled Loading Situations for the Example Problems

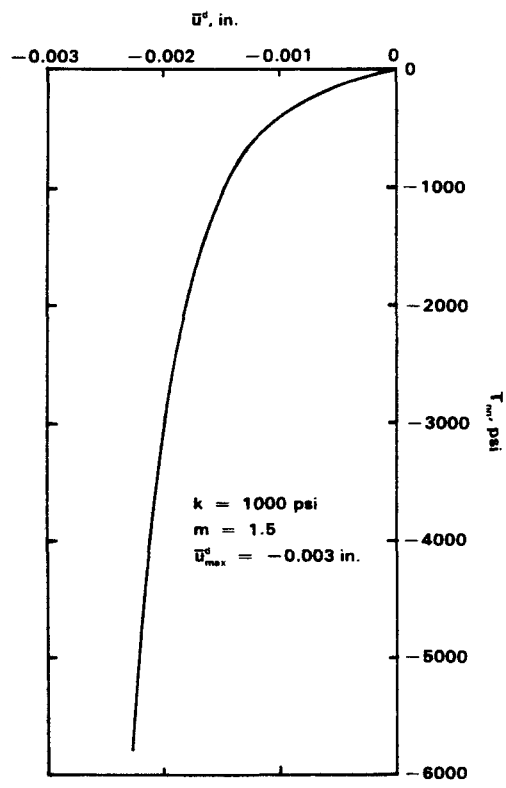

Figure 6. Joint Normal Stiffness Used for Example 1

For the initial conditions, we arbitrarily assume

$$\underset{\approx}{\varepsilon} = \underset{\approx}{0}$$
$$\sigma_{11} = \sigma_{22} = \sigma_{33} = -200 \text{ psi}$$
$$\sigma_{12} = \sigma_{23} = \sigma_{31} = 0$$
$$\bar{u}^d = -0.000765 \text{ in.}$$
$$\bar{u}^s = 0$$

This is a pure nonlinear elastic problem since all shear components are identically zero. Results are shown in Figure 7 for selected values of joint spacing δ. Clearly, as δ becomes large, the effect of joint dilation becomes less significant until only the linear block response of the intact material is observed. Changes in the initial fracture permeability parallel to jointing is based on Eq (48), and is shown in Figure 8. Order-of-magnitude changes may be expected. The permeability changes are the greatest for the large joint spacings, but these initial fracture permeabilities are quite small so the changes may be insignificant.

Shear Response Without Coupled Displacements

Consider now the reduced problem,

$$e_{22} = 0.0015$$

$$e_{11} = e_{33} = e_{23} = e_{31} = 0$$

and e_{12} being variable. As in the previous example, let

$$\underset{\sim}{n} = (0,1,0)^T$$

so the stress σ_{12} measures the response to pure shear strains. The material properties and initial conditions are the same as before. In addition, the single-joint shear modulus is selected to be

$$G_s = 0.1 \times 10^6 \text{ psi}$$

and the slip function is selected to be

$$\mu = 0.7$$
$$\text{Co} = 250 \text{ psi.}$$

The calculated cyclic shear stress-shear strain response is shown in Figure 9 for various joint spacings. Because the normal strain e_{22} is held constant, the normal stress σ_{22} and hence the flow stress will vary with the joint spacing (δ). As the joint spacing (δ) increases, the initial modulus approaches the intact material modulus and the flow stress increases to infinity.

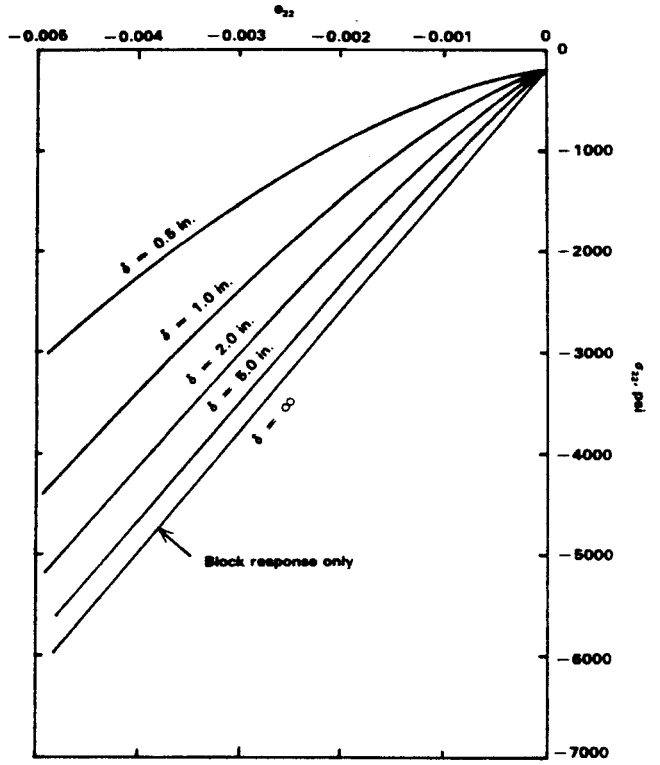

Figure 7. Stress-Strain Response Normal to Jointing for Example 1

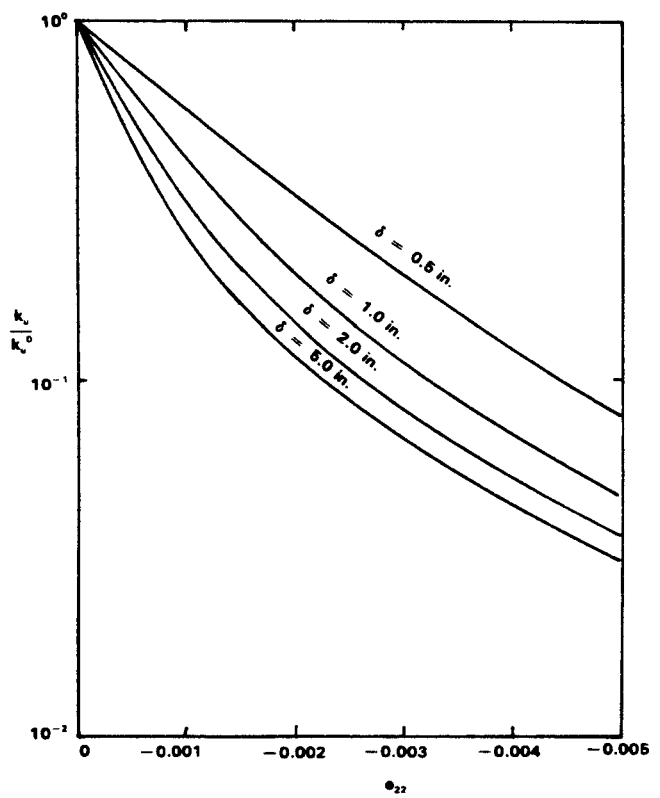

Figure 8. Effect of Joint Normal Strain on Fracture Permeability Parallel to Jointing for Example 1

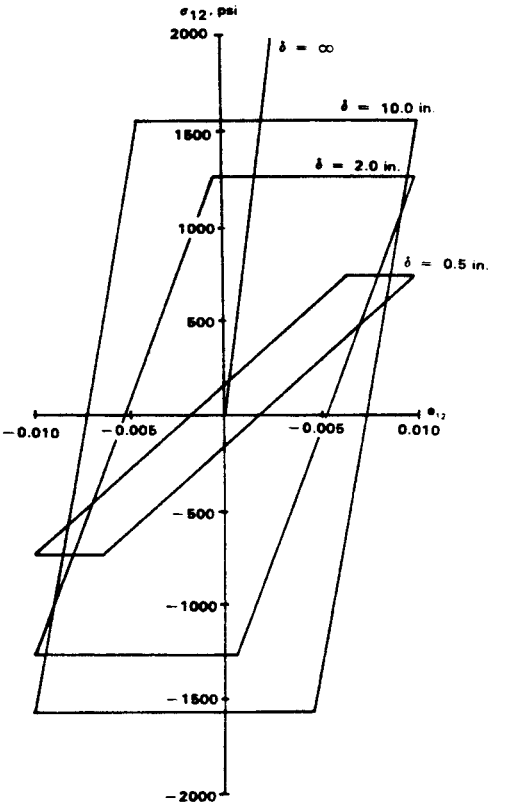

Figure 9. Stress-Strain Response in Shear Parallel to Jointing for Example 2

Shear Response With Coupled Displacements

This problem is the same as the previous example, except that coupled dilation displacements are included. During shear strain loading, the dilation displacement increases as does the normal stress T_{nn}. This is shown in Figure 10 for three dilation angles. For ψ = 10°, the normal stress increases to such an extent that shear slippage is prevented. The shear stress-strain

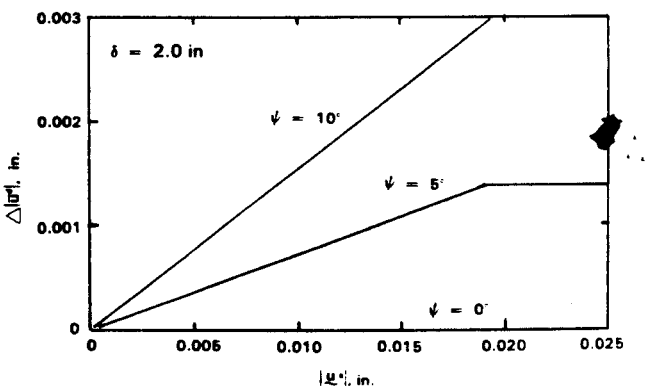

Figure 10a. Effect of Coupled Dilation Angle on Joint Normal Displacement for Example 3

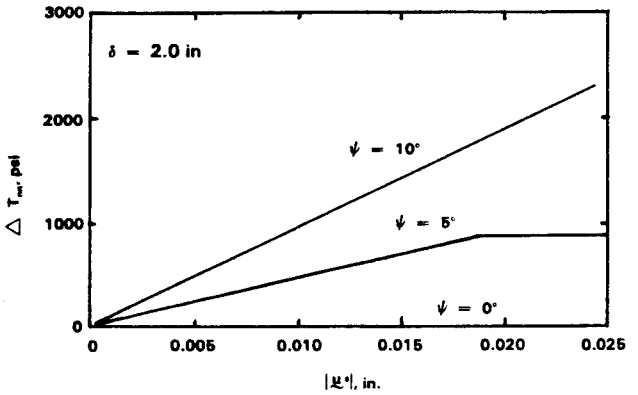

Figure 10b. Effect of Coupled Dilation Angle on Joint Normal Stress for Example 3

curves shown in Figure 11 show how the flow stress increases with the dilation angle. Finally, the results in Figure 12 show that the flow permeability parallel to jointing can be increased several orders of magnitude by coupled dilation displacements.

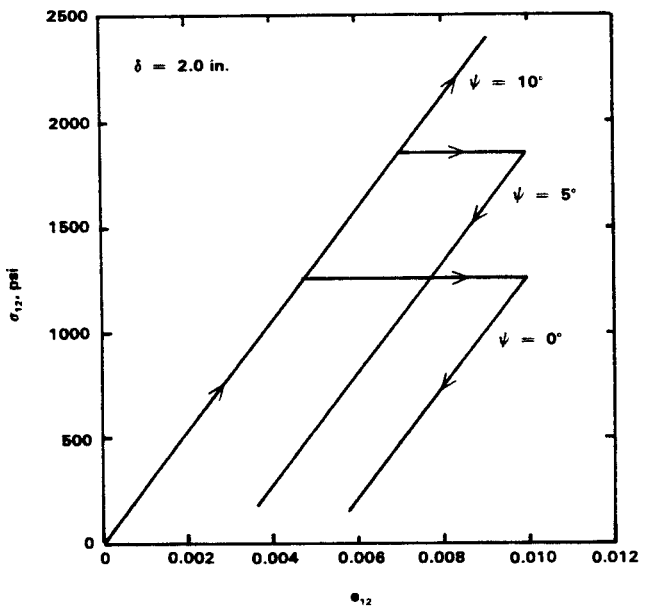

Figure 11. Effect of Coupled Dilation Angle on Flow Stress for Example 3

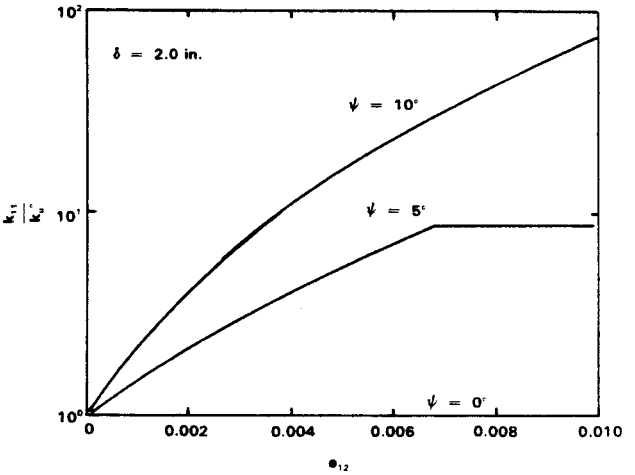

Figure 12. Effect of Coupled Dilation Angle on Fracture Permeability Parallel to Jointing for Example 3

Future Work

It is recognized that the continuum approximation presented in this report represents only a first step toward modelling the behavior of a jointed rock mass. Much additional work, both analytical and experimental, is necessary before a realistic model is achieved. The following is a partial list of remaining development work:

1. Experimental data on single-joint specimens are required not only to quantify material constants, but to define the functional form of the joint stiffness equations given by Eq (26).
2. The strain decomposition [Eq (30)] should permit additional jointing planes, since the joint systems observed in the field are usually present in three orthogonal sets.
3. For some applications, a large strain formulation will be necessary.
4. This model will have limited usefulness unless large-scale verification tests are performed. Several have been performed and reported in the literature. These should be investigated with respect to potential verification of this continuum model.

References

[1]P. A. Witherspoon et al, "New Approaches to Problems of Fluid Flow in Fractured Rock Masses," *Proc. 22nd Symp. Rock Mechanics,* MIT, June 28-July 2, 1981.

[2]L. W. Morland, "Continuum Model of Regularly Jointed Mediums," *J Geophys Res,* Vol 79, No. 2, 1974, pp 357-362.

[3]L. W. Morland, "Elastic Response of Regularly Jointed Media," *Geophys J,* Vol 37, 1974, pp 435-446.

[4]L. W. Morland, "Plane Wave Propagation in Anisotropic Jointed Media," *Q J Mech and Appl Math,* Vol 30, 1977, pp 1-21.

[5]R. E. Goodman, *Methods of Geological Engineering* (St. Paul, MN: West Pub. Co., 1976).

[6]Personal communication, S. P. Neuman, Univ. of Arizona, Tucson, Arizona, March 1981.

2nd Distribution:
1521 R. K. Thomas (100)
TID-4500-R69 UC-70 (325)

US Department of Energy
Office of Waste Isolation
Room B-207
Germantown, MD 20767
Attn: C. A. Heath, Director

US Department of Energy
Technology Team
Room B-220
Germantown, MD 20767
Attn: D. L. Vieth, Acting Team Leader

US Department of Energy
National Waste Terminal Storage Program Office
505 King Ave.
Columbus, OH 43201
Attn: J. O. Neff, Program Manager

Lawrence Livermore National Laboratory
University of California
PO Box 808
Mail Stop L-204
Livermore, CA 94550
Attn: L. D. Ramspott, Tech Project Officer

Los Alamos National Laboratory
University of California
PO Box 1663
Mail Stop 514
Los Alamos, NM 87545
Attn: B. R. Erdal, Tech Project Officer

Westinghouse - AESD
PO Box 708
Mail Stop 703
Mercury, NV 89023
Attn: A. R. Hakl, Site Manager

US Geological Survey (2)
PO Box 25046
Mail Stop 954
Federal Center
Denver, CO 80301
Attn: G. L. Dixon, Tech Project Officer
W. E. Wilson

Sandia National Laboratories
PO Box 14100
Organization 4764
Las Vegas, NV 89114
Attn: A. E. Stephenson, Tech Overview Management

W. S. Twenhofel
820 Estes Street
Lakewood, CO 80226

US Department of Energy
Office of Waste Isolation
Room B-214
Germantown, MD 20767
Attn: C. R. Cooley, Deputy Director

US Department of Energy
Richland Operations Office
PO Box 550
Richland, WA 99352
Attn: R. G. Goranson

Rockwell International Atomics
International Division
Rockwell Hanford Operations
Richland, WA 99352
Attn: R. Deju

US Department of Energy (3)
Waste Management Project Office
PO Box 14100
Las Vegas, NV 89114
Attn: R. M. Nelson, Jr., Director

US Department of Energy
Office of Public Affairs
PO Box 14100
Las Vegas, NV 89114
Attn: D. F. Miller, Director

US Department of Energy
CP-1, M/S 210
PO Box 14100
Las Vegas, NV 89114
Attn: R. H. Marks

US Department of Energy
Health Physics Division
PO Box 14100
Las Vegas, NV 89114
Attn: B. W. Church, Director

US Department of Energy (7)
PO Box 14100
Las Vegas, NV 89114
Attn: R. R. Loux

DISTRIBUTION (cont):

Holmes & Narver, Inc.
PO Box 14340
Las Vegas, NV 89114
Attn: A. E. Gurrola

Lawrence Livermore National Laboratory
University of California
Mail Stop L-209
PO Box 808
Livermore, CA 94550
Attn: K. Street, Jr.

Los Alamos National Laboratory
Mail Stop 760
PO Box 1663
Los Alamos, NM 87545
Attn: D. C. Hoffman

Battelle
Office of NWTS Integration
505 King Ave.
Columbus, OH 43201
Attn: W. A. Carbiener

Battelle (7)
Office of Nuclear Waste Isolation
505 King Ave.
Columbus, OH 43201
Attn: N. E. Carter
S. Goldsmith
ONWI Library (5)

State of Nevada
Governor's Office of Planning Coordination
Capitol Complex
Carson City, NV 89023
Attn: R. M. Hill, State Planning Coordinator

State of Nevada
Department of Energy
Capitol Complex
Carson City, NV 89710
Attn: N. A. Clark

International Atomic Energy Agency
Division of Nuclear Power & Reactors
Karnter Ring 11
PO Box 590, A-1011
Vienna, AUSTRIA
Attn: J. P. Colton

Reynolds Electrical & Engineering Co., Inc.
Mail Stop 555
PO Box 14400
Las Vegas, NV 89114
Attn: H. D. Cunningham

Fenix & Scisson, Inc.
PO Box 15408
Las Vegas, NV 89114
Attn: J. A. Cross

Argonne National Laboratories
9700 S. Cass Ave.
Argonne, IL 60439
Attn: A. M. Friedman

1112 C. R. Mehl
Attn: C. W. Smith
1112 A. J. Chabai
1417 F. W. Muller
4760 R. W. Lynch
4761 L. W. Scully
4762 L. D. Tyler
4762 R. R. Peters
4763 J. R. Tillerson
4763 A. R. Lappin
4764 R. C. Lincoln
5500 O. E. Jones
5510 D. B. Hayes
5511 J. W. Nunziato
5520 T. B. Lane
5521 J. H. Biffle
5521 D. P. Flanagan
5521 N. D. Gilbertsen
5521 R. D. Krieg
5521 C. M. Stone

DISTRIBUTION (cont):

5521 D. V. Swenson
5521 R. K. Thomas (15)
5522 T. G. Priddy
5522 R. L. Johnson
5522 K. W. Schuler
5522 R. K. Wilson
5524 L. W. Davison
5530 W. Herrmann
5532 B. M. Butcher
5532 D. J. Holcomb
5532 W. A. Olsson
5532 R. H. Price
5532 L. W. Teufel
5532 W. R. Wawersik
5541 W. C. Luth
8120 L. D. Bertholf
8214 M. R. Pound
3141 L. J. Erickson (5)
3151 W. L. Garner (3)